Quantum grow—A quantum dynamics sampling approach for growing potential energy surfaces and nonadiabatic couplings

Oded Godsi,[1] Michael A. Collins,[2] and Uri Peskin[1,a)]
[1]*Schulich Faculty of Chemistry and The Lise Meitner Center for Computational Quantum Chemistry, Technion-Israel Institute of Technology, Haifa 32000, Israel*
[2]*Research School of Chemistry, Australian National University, Canberra, Australian Capital Territory 0200, Australia*

(Received 10 January 2010; accepted 22 February 2010; published online 25 March 2010)

A quantum sampling algorithm for the interpolation of diabatic potential energy matrices by the Grow method is introduced. The new procedure benefits from penetration of the wave packet into classically forbidden regions, and the accurate quantum mechanical description of nonadiabatic transitions. The increased complexity associated with running quantum dynamics is reduced by using approximate low order expansions of the nuclear wave function within a Multi-configuration time-dependent Hartree scheme during the Grow process. The sampling algorithm is formulated and applied for three representative test cases, demonstrating the recovery of analytic potentials by the interpolated ones, and the convergence of a dynamic observable. © *2010 American Institute of Physics*. [doi:10.1063/1.3364817]

I. INTRODUCTION

To simulate the dynamics of a molecular system during reaction, potential energy surfaces (PESs) and often nonadiabatic coupling terms need to be known for large numbers of molecular configurations.[1] These can be calculated using modern quantum chemical methods,[2] either prior to the dynamics simulation or "on-the-fly," during the dynamics.[3] However, as the computational cost of *ab initio* calculations rises steeply with the demand for accuracy, and with the number of electrons, compromises are usually made between the cost and the quality of the PES and hence most dynamics simulations are based on approximated PES.

Approximated PES can be generated by fitting or by interpolation approaches. The differences between the fitted or interpolated potential and the (unknown) *ab initio* potential are another source of error in observables calculation which needs to be minimized. In a traditional fitting approach[1,4] the PES is expressed as a combination of functional forms, and the details of the combination are determined by minimizing the fitting error over a set of geometries at which the *ab initio* energy is known (a training set). Among the interpolating approaches, modified Shepard interpolation[5–8] has a number of attractive features: the approach involves only a handful of fixed parameters, the method is local in nature, and the quality of the interpolated PES can be easily and systematically improved by adding more data. In recent papers the modified Shepard interpolation was extended for constructing PES for diabatic processes which involve more then one PES.[9–11]

While the cost of the interpolation is set by the number of *ab initio* sampling points, the quality of the approximation depends also on the distribution of these sampling points in the molecular configurations space. Moreover, considering that different experimental (and the corresponding computational) observables often sample different regions of the PES, different molecular configurations are required for different observables. An economic sampling of the PES should take into consideration the observables of interest during the selection process of a set of most relevant sampling points. A common approach for associating the sampling points with the desired observable is to relate the sampling to the dynamics of the system for a relevant set of initial conditions. In the Grow method[12] new data points are sampled according to their occurrence in classical trajectories, run on an approximate PES based on existing data points. The resulting interpolated potential is constructed iteratively until convergence is obtained for the required observables.

In this work we explore the possibility of extending the Grow method by using "quantum sampling," that is, replacing the classical dynamics in the grow process by a corresponding approximated quantum dynamics. Quantum sampling is expected to be superior to classical sampling when light atoms are involved and when multiple PESs contribute significantly to the dynamics, where the observables reflect inherent quantum dynamics. Nevertheless, exact quantum dynamics is more computationally demanding, due to its exponential scaling with the number of coupled nuclear degrees of freedom. This suggests that exact quantum dynamics simulations during the grow process would make it impractical, and it is therefore proposed here to apply approximate quantum dynamics for the sampling steps. The multiconfiguration time-dependent hartree (MCTDH) approach[13–17] is a numerically exact approach based on a set of converging approximations. MCTDH-calculations have already been applied in calculations involving Shepard interpolated PESs[18,19] and were used to monitor the convergence of the grow process[20] In this work we propose to use the MCTDH method for the quantum sampling process. Using low order expansions with only weak correlation an approxi-

a)Electronic mail: uri@techunix.technion.ac.il.

mated quantum dynamics is obtained for a modest numerical effort which makes this approach attractive for this purpose.

The paper is set out as follows. The modified Shepard interpolation method is presented briefly in Sec. II. Section III describes the new modification of the grow method, using quantum sampling, and in Sec. IV this new approach is demonstrated for three examples. The first example represents a single PES in a one-dimensional configuration, the second example involves dynamics on two coupled electronic states, and the last example is the nonadiabatic process, $Na^*+H_2 \rightarrow Na+H_2$, described by an analytic potential of the three bodies on two coupled electronic states, involving a conical intersection. Concluding remarks are presented in the last section.

II. MODIFIED SHEPARD INTERPOLATION

The modified Shepard interpolation approach is described in details elsewhere,[5–8,12] and only a short description is given here. The method is based on transforming the PES and the corresponding nonadiabatic couplings to a quasidiabatic representation.[9–11,21–25] The diabatic potential energy matrix (DPEM), such as the PES, is a smooth function of the nuclear coordinates and hence can be expanded locally as a Taylor series. Globally, the DPEM is constructed as a weighted sum of Taylor expansions from a scattered set of geometries called "data points." An internal molecular geometry is defined by a transformation of the atomic Cartesian coordinates $\mathbf{X}$ into inverse pair distances, whose number for a system of N atoms is $N_{int}=N(N-1)/2$. Denoting the coordinates representing the internal molecular geometry as $\mathbf{z}$, the corresponding DPEM is calculated as

$$\underline{\underline{D}}(\mathbf{z}) = \sum_{g\in G}\sum_{n=1}^{N_{\text{data}}} w(\mathbf{z};\mathbf{z}(g\circ n))\underline{\underline{D}}(\mathbf{z};\mathbf{z}(g\circ n)). \tag{2.1}$$

$\underline{\underline{D}}(\mathbf{z})$ is a $N_s\times N_s$ matrix (N_s is the number of adiabatic electronic PES), constructed as a weighted sum. Each element in $\underline{\underline{D}}(\mathbf{z};\mathbf{z}(g\circ n))$ is a (second order) Taylor series in $\mathbf{z}$ centered at a specific molecular configuration (data point), $\mathbf{z}(g\circ n)$, so that

$$\begin{aligned} D_{i,j}(\mathbf{z};\mathbf{z}(g\circ n)) = {} & D_{i,j}[\mathbf{z}(g\circ n)] \\ & + \sum_{l=1}^{N_{\text{int}}} \left.\frac{\partial D_{i,j}[\mathbf{z}]}{\partial z_l}\right|_{\mathbf{z}(g\circ n)} [z_l - z(g\circ n)_l] \\ & + \frac{1}{2}\sum_{l_1=1}^{N_{\text{int}}}\sum_{l_2=1}^{N_{\text{int}}} \left.\frac{\partial^2 D_{i,j}[\mathbf{z}]}{\partial z_{l_1}\partial z_{l_2}}\right|_{\mathbf{z}(g\circ n)} \\ & \times [z_{l_1} - z(g\circ n)_{l_1}][z_{l_2} - z(g\circ n)_{l_2}], \end{aligned} \tag{2.2}$$

and $\mathbf{z}(g\circ n)\equiv g\circ\mathbf{z}(n)$ is the configuration obtained by acting on some particular (numbered) data point $\mathbf{z}(n)$, with an element g of the molecular symmetry group G, here G is the complete nuclear permutation inversion group.

The weights $w(\mathbf{z};\mathbf{z}(g\circ n))$ can be viewed as a probabilistic estimate of the accuracy of each local Taylor series in the interpolation. This naturally leads to a number of conditions placed on the weights, such as the constraint that the weights must sum to unity. A simple form for the weight function that satisfies these requirements is given by

$$w(\mathbf{z};\mathbf{z}(g\circ n)) = \frac{v(\mathbf{z};\mathbf{z}(g\circ n))}{\sum_{g\in G}\sum_{m=1}^{N_{\text{data}}} v(\mathbf{z};\mathbf{z}(g\circ m))}. \tag{2.3}$$

$v(\mathbf{z};\mathbf{z}(g\circ n))$ is called the "primitive weight" and it is usually a function of the internal coordinate distances. In simple terms, we can say that $v(\mathbf{z};\mathbf{z}(g\circ n))$ is larger as $\mathbf{z}(g\circ n)$ is "closer" to $\mathbf{z}$.

III. QUANTUM SAMPLING

In this section we focus on the selection of data points for the modified Shepard interpolation. There are several advantages for running quantum instead of classical dynamics simulations for this purpose, among them are the accessibility of the sampling to classically forbidden regions (through quantum tunneling), the absence of zero point energy artifacts, description of nonadiabatic transitions beyond the surface hopping algorithm,[26] and consistency with quantum calculations of dynamical observables. The ability to perform exact quantum mechanical simulations on multidimensional PES is limited in practice, however, due to the exponential scaling with the number of nuclear degrees of freedom. It is therefore proposed to sample the data points according to approximated quantum simulations. The MCTDH method by the Heidelberg group[13–17] is an optimal framework for this purpose. The approach is based on expanding the many body time-dependent wave functions as a sum of products (configurations) of single particle functions. Using variationally optimized time-dependent single particle functions, the number of required configurations and the number of single particle functions are minimized. For the data points sampling process, an approximated function is sufficient, i.e., a small number of single particle functions is sufficient to get a reliable description of the molecular configuration space. For observables calculations, the number of single particle functions and the number of configurations can be systematically increased till convergence of the required observable.

Selection of data points according to quantum evolution can be carried out in different ways. A favorable strategy that was adopted below is to search for nuclear configurations associated with the highest probability density along the time evolution. Notice that the although the MCDTH wave function representations in terms of single particle functions has a favorable scaling with the number of degrees of freedom, the construction of the multidimensional probability density scales exponentially, in principle. Nevertheless, the products form of the MCTDH wave function can be utilized to perform an efficient search for the maximally populated points in the nuclear configuration space using multiresolution analysis which does not require the construction of the entire wave function. In this work we consider explicitly the cases in which the construction of the multidimensional wave function is not the limiting computational step.

For implementing the quantum sampling using the MCTDH method, we choose to discretize the space of internal nuclear coordinates (inverse pair distances), where $\mathbf{z}_j$

$=z_{1,j},z_{2,j},\ldots,z_{N(N-1)/2,j}$ denotes a single grid point. The full time-dependent wave function is given as

$$\Psi(\mathbf{z}_j,t_i)=\sum_{s=1}^{N_s}\phi_s(\mathbf{z}_j,t_i)|s\rangle, \tag{3.1}$$

where $|s\rangle$ is an adiabatic electronic state and $\phi_s(\mathbf{z}_j,t_i)$ is the corresponding nuclear wave function at time t_i. For each state and each grid point the maximal probability density during the time evolution is recorded and denoted as $P_j^{\max}$

$$P_j^{\max}\equiv\max\left[\sum_s|\phi_s(\mathbf{z}_j,t_i)|^2\right]. \tag{3.2}$$

The points associated with the highest values of $P_j^{\max}$ are considered as a list of candidates for sampling as data points. The criterion for selecting a point $\mathbf{z}_l$ into this list is

$$P_l^{\max}>p\max_j\{P_j^{\max}\}, \tag{3.3}$$

where $0<p<1$. In the simulations described below, p was typically chosen around $p\approx0.02$. From this list of points, $\{\mathbf{z}_l\}$; $l=1,2,\ldots,N_l$, a new data point is added to the existing data points according to the criteria listed below. These criteria are based on the algorithm for classical sampling, published elsewhere.[11,12] Here we highlight some differences from the classical sampling algorithm.

1. *h -weight*: Each point in the list is ranked according to the following formula:

$$h[\mathbf{z}_l]=\frac{1}{N_l-1}[P_l^{\max}]^q\left(\sum_{g\in G}\sum_{n=1}^{N_{\text{data}}}(\mathbf{z}_l-g\circ\mathbf{z}(n))^{-2p}\right)^{-1}, \tag{3.4}$$

where p is a positive integer larger than $3N-6$,[12] that damps the score of points in the list that are close to existing data points. The value of q affects the dependence of the score on the maximal probability density of each point. Large values favor points with large probability density. During the growing process, the value of q is systematically reduced toward 0, so that the h-weight is not affected by the probability density, allowing for sampling of classically forbidden regions in which the probability density is inherently small. (Notice that the denominator is also changed during the growing process when each data point is assigned confidence radii.[12]) The point $\mathbf{z}_l$ with the largest score of h (denoted as $\mathbf{z}_h$) is chosen as a new data point, i.e.,

$$h(\mathbf{z}_h)=\max_l(h(\mathbf{z}_l)). \tag{3.5}$$

2. *Variance sampling:* Each point in the list, $\{\mathbf{z}_l\}$; $l=1,2,\ldots,N_l$, is inspected to see if adding it as a data point would improve the accuracy of the interpolation. Denoting the DPEM obtained by the full set of data points, and by a single data point as $\underline{\underline{D}}(\mathbf{z}_l)$ and $\underline{\underline{D}}(\mathbf{z}_l;\mathbf{z}(g\circ n))$, respectively, [see Eqs. (2.1) and (2.2)], noticing that $\underline{\underline{D}}(\mathbf{z}_l)$ is a weighted average of $\{\underline{\underline{D}}(\mathbf{z}_l;\mathbf{z}(g\circ n))\}$, the variance in the interpolation at $\mathbf{z}_l$ of a matrix element $\underline{\underline{D}}_{i,j}(\mathbf{z}_l)$ is defined as

$$\sigma_{i,j}^2[\mathbf{z}_l]=\sum_{g\in G}\sum_{n=1}^{n\text{data}}w(\mathbf{z}_l;\mathbf{z}(g\circ n))[\underline{\underline{D}}_{i,j}(\mathbf{z}_l;\mathbf{z}(g\circ n))-\underline{\underline{D}}_{i,j}(\mathbf{z}_l)]^2. \tag{3.6}$$

Statistically, the larger the value of the variance, the more unlikely it is for the interpolation to be accurate. Therefore points from the list get higher score for high variance value. The off-diagonal coupling terms of the DPEM are usually much smaller in magnitude than the diagonal terms. It is therefore instructive to calculate the variance of the diagonal and the off-diagonal terms separately, defining

$$\sigma_{\text{diag}}^2[\mathbf{z}_l]=\sum_{i=1}^{N_s}\sigma_{i,i}^2[\mathbf{z}_l];\quad\sigma_{\text{off-diag}}^2[\mathbf{z}_l]=\sum_{i=1}^{N_s}\sum_{j\neq i}^{N_s}\sigma_{i,j}^2[\mathbf{z}_l]. \tag{3.7}$$

The two points with the highest variance values, denoted as $\mathbf{z}_{\text{diag}}$ and $\mathbf{z}_{\text{off-diag}}$, are chosen as new data points, i.e.,

$$\sigma_{\text{diag}}^2(\mathbf{z}_{\text{diag}})=\max[\sigma_{\text{diag}}^2(\mathbf{z}_l)];$$
$$\sigma_{\text{off-diag}}^2(\mathbf{z}_{\text{off-diag}})=\max[\sigma_{\text{off-diag}}^2(\mathbf{z}_l)]. \tag{3.8}$$

The quantum sampling procedure is embedded in the following MCTDH-based quantum mechanical grow algorithm:

1. Chose a set geometries as an initial set of data points. These points should represent the chemically important regions in configuration space, typically the reactants, products, a saddle point, and some configurations on a minimum energy path for the reaction. For each initial data point, calculate the electronic energy, its first and second derivatives in all directions, the derivative coupling, and its first derivative in all directions.[11]
   For the construction of the *ab initio* DPEM some additional initial *ab initio* investigation is required. In particular, at least one molecular configuration near a conical intersection must be determined and included in the initial data set. At this geometry, multireference *ab initio* calculation yields the adiabatic energies of the relevant states and the derivative coupling between them.
   Using the methods of Ref. 11, evaluate the matrices that determine the symmetry of the DPEM, and an initial estimate of the adiabatic-to-diabatic (ADT) transformation matrices for the data set,[11] and go to step (3) below.
2. For each new data point, perform an electronic structure calculation of the electronic energy, its first and second derivatives in all directions, the derivative coupling, and its first derivative in all directions.[11]
3. Update the ADT matrices according to new data points using a consistency constraint to establish a smooth diabatic representation,[11] and use it to calculate the DPEM for a discrete representation in a selected coordinate system (Jacobi, Cartezian, etc).
4. Approximate each element of the DPEM matrix as sums of products in the different coordinates (natural expansion). This step is carried out using the "POTFIT" procedure in the MCTDH package.[16]

5. Choose an initial quantum wave packet and the time propagation parameters.
6. Run an approximate quantum propagation using MCTDH.
7. Calculate observables of choice from the time-dependent wave function.
8. If observables are converged go to step 11.
9. Select new data points according to the quantum sampling algorithm described above.
10. Go to step 2.
11. Stop.

IV. ILLUSTRATIVE NUMERICAL EXAMPLES

To illustrate the convergence of the quantum sampling algorithm three representative test cases were considered, for which the DPEM (or the potential) is analytically known. The first is a one-dimensional adiabatic process involving tunneling through a barrier in a double well potential, and the second is a nonadiabatic process involving a single nuclear coordinate and two coupled electronic states. These two model cases are given in order to illustrate the efficiency of quantum sampling in cases where quantum effects dominate the dynamics.[27] The third test is for a more complex nonadiabatic process, $Na^*+H_2 \rightarrow Na+H_2$, involving three internal nuclear coordinates and two electronic states with a conical intersection. In this case required *ab initio* inputs were constructed artificially from the analytic DPEM, following the procedure described in Ref. 11.

In each case, the observables were selected to be the autocorrelation function, $C(t)=\langle\psi(0)|\psi(t)\rangle$, and its Fourier transform (the autocorrelation spectrum) $S(E)=\lim_{t\to\infty}(1/2\pi)\int_{-t}^{t}dt' e^{-iEt'}C(t')$. To demonstrate that the convergence of these observables during the quantum mechanical growing procedure is due to the convergence of the interpolated potential, the error in the interpolated potential with respect to the analytically known values was followed. The error was defined for a set of points, selected by running a wave packet using the analytic DPEM and selecting the points with maximal $P_l^{\max}$ values, $\{\mathbf{z}_l\}$; $l=1,2,\ldots,N_l$, i.e., the points with the highest probability density during the time evolution. For this list of points the error was calculated and averaged as follows after each iteration of the quantum grow algorithm:

$$\langle\Delta\rangle \equiv \frac{1}{N_l}\sqrt{\sum_{l=1}^{N_l}\sum_{n=1}^{N_s}[E_n(\mathbf{z}_l)-E_n^{(\text{exact})}(\mathbf{z}_l)]^2}, \tag{4.1}$$

where $E_n^{(\text{exact})}(\mathbf{z}_l)$ and $E_n(\mathbf{z}_l)$ are the eigenvalues of the analytic and the interpolated DPEM at the point $\mathbf{z}_l$, respectively.

A. A one-dimensional tunneling barrier

The first example considered was a particle (of mass 2000 a.u.) in an analytic non symmetric double well potential

$$V_1(x) = 0.01(x-5)^4 - 0.05(x-4.9)^2. \tag{4.2}$$

A single initial data point was set near the left well minimum, located at $x_0=3.5$, introducing an initial interpolated potential of a single harmonic well. The initial wave packet was taken to be a nonstationary Gaussian, centered at x_0, with an average momentum $k_x=9$ and a standard deviation in position $\sigma_x=0.4$ (all in a.u.). The wave packet was sampled on a discrete equally spaced grid with, $N_x=512$ $X_{\min}=2$ $X_{\max}=8$, and propagated using the Fourier split operator method.[28,29]

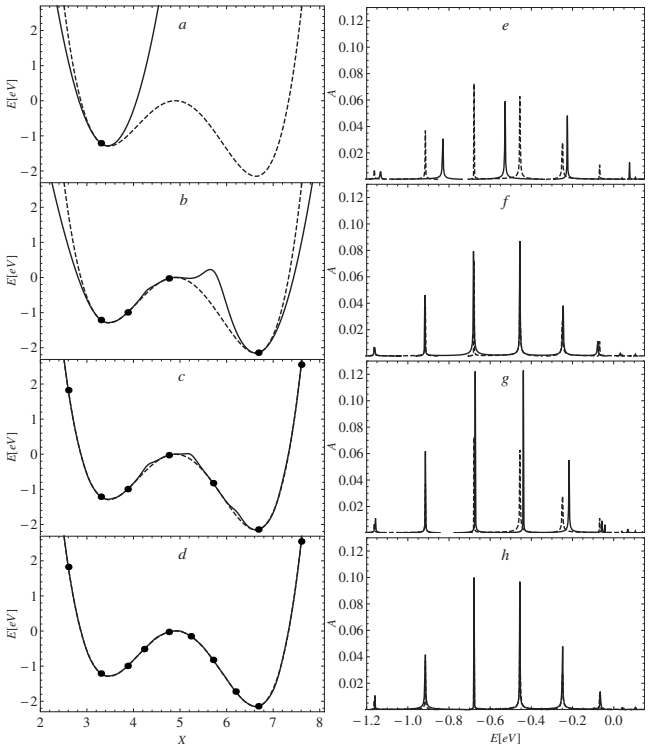

FIG. 1. Left column: An analytic double well potential (dashed) and its interpolated approximation (solid) with 1, 4, 7, and 10 sampling points corresponding to plots a, b, c, and d, respectively. Right column: Corresponding autocorrelation spectra, obtained using the analytic (dashed) and the interpolated (solid) potential respectively after propagation time of 30 000 a.u. e, f, g, and h correspond to the potentials a, b, c, and d, respectively.

In each grow iteration the quantum sampling method with $p=0.005$ was used to select new data points. Figure 1 compares the interpolated potential with 1, 4, 7, and 10 data points along with the data points positions. As can be seen the interpolated potential with 10 data points is converged to the analytic double well potential. Notice that a fast convergence is facilitated by the penetration of the quantum wave packet into the classically forbidden region, which accelerates the sampling of the barrier and the right well regions of the potential. The corresponding autocorrelation spectrum, $S(E)$ calculated on the interpolated potentials, is shown to converge to the calculation based on the analytical potential. In Fig. 2 the sharp decrease in the potential interpolation error with every new data point is demonstrated.

B. Two coupled surfaces

Here we study a DPEM which resembles that of the two lowest electronic states of an alkali-hydrogen molecule, MH, M=Li, Na, K, Cs at zero total angular momentum, $J_{\text{tot}}=0$ (Ref. 30). One of the diabatic states is of ionic character and supports bound states and the other is of a covalent char-

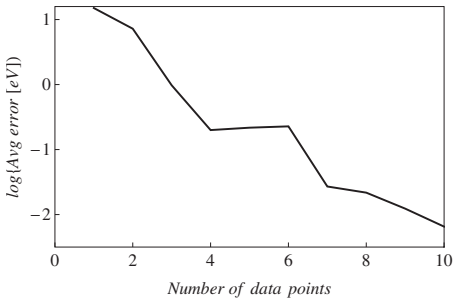

FIG. 2. The average error between the interpolated and the analytic potential [$\langle\Delta\rangle$ of Eq. (4.1)] for the one-dimensional double well potential.

acter and repulsive. At short bond distances the ionic state is lower in energy but as the interatomic distance increases, the two diabatic potentials cross, i.e., the ground state at large distances corresponds to the neutral atoms. The DPEM elements read (energies in hartrees and distances in a.u.)

$$V_{11}(x) = 0.11(1 - \exp[-0.33(x-4.5)])^2 - 0.70,$$

$$V_{12}(x) = 0.015(\exp[-0.1(x-8.83)^2]), \qquad (4.3)$$

$$V_{22}(x) = \exp[-0.02(x+7)^2] - 0.64,$$

where V_{11} is a Morse potential, V_{12} is a Gaussian, and V_{22} is a repulsive potential. The potential was sampled using a uniform grid, with the following parameters, $nx=1024$ $X\,\min=0.5$ $X\,\max=50$. To absorb the wave function at the finite grid boundaries a complex absorbing potential (CAP) $-iW(x)$ was added to the corresponding adiabatic potentials, $W(x)=\eta|x-x_c|^b\Theta[(x-x_c)]$, where Θ is the Heaviside's step function, and the CAP parameters chosen as, $x_c=40$, $\eta=0.04$, and $b=4$.

The initial data set contained 2 data points, one near the minimum of V_{11} at $x=3$, and the other at the asymptote at $x=40$. The initial wave packet for the quantum grow process was chosen as a Gaussian, centered at the asymptote around $x_0=35$, with an average momentum, $k_x=5$ and a standard deviation in position, $\sigma_x=1.0$ (all in a.u.) restricted to the adiabatic ground state. The time evolution of the atomic collision process was followed using the split operator propagation method.[28,29] In each run the wave packet were propagated for a time of 90 000 a.u. using a time step $dt=5$ a.u. New data points were added using the quantum sampling method with $p=0.01$.

Figure 3 compares the progression of the interpolated DPEM elements, demonstrating convergence to the analytic potential for 19 data points. The corresponding convergence of the autocorrelation spectrum obtained by propagating a Gaussian wave packet, initially localized in the lower adiabatic potential well ($x_0=6.7$ a.u., $k_x=0$ a.u., and $\sigma_x=1.0$ a.u.) on the interpolated potentials to the spectrum obtained with the analytic potential is also demonstrated. Figure 4 displays the average error as a function of the number of data points, where it can be seen that the average error decreases sharply with every new data points.

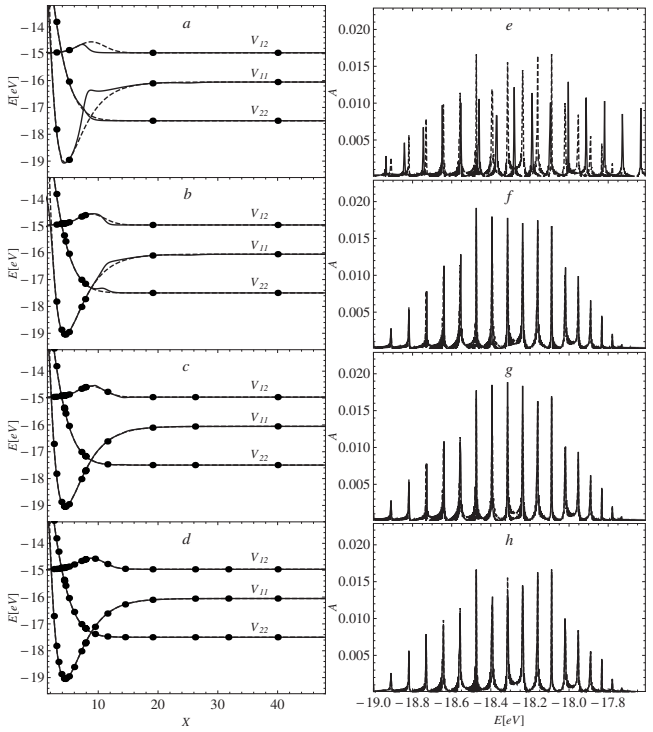

FIG. 3. Left column: Analytic DPEM matrix elements for two coupled surfaces (dashed) and their interpolated approximation (solid) with 4, 9, 14, and 19 sampling points corresponding to plots a, b, c, and d, respectively (V_{12} was shifted to fit the plot). Right column: Corresponding autocorrelation spectra, obtained using the analytic (dashed) and the interpolated (solid) DPEMs, respectively, after propagation time of 90 000 a.u. e, f, g, and h correspond to the potentials a, b, c, and d, respectively.

C. Dynamics through a conical intersection

The analytic model used here for the system, $Na^*+H_2 \rightarrow Na+H_2$, is based on a London-Eyring-Polanyi-Sato (LEPS) PES proposed by Truhlar *et al.*[31–33] This fitted potential predicts the existence of a deep and narrow well in the excited PES ($V_{22}(Rd,Rv,\theta)$) near the C_{2v} symmetry of the three atoms system, i.e., at $\theta \approx \pi/2$, or $\sphericalangle NaH_1H_2 \cong \sphericalangle NaH_2H_1$ (see Fig. 5). To investigate this feature of the surfaces, the MOLPRO program[34] was used to evaluate the multireference configuration-interaction (MRCI) energies of the two lowest energy adiabatic states, using the 6−311++G(2df,2pd) Pople basis set, based on a three-state-averaged (equal weights) multiconfiguration self-consistent field wave function. In this region, the MRCI calculations reveal only a very mild decrease in V_{22} near C_{2V} symmetry. Therefore, the

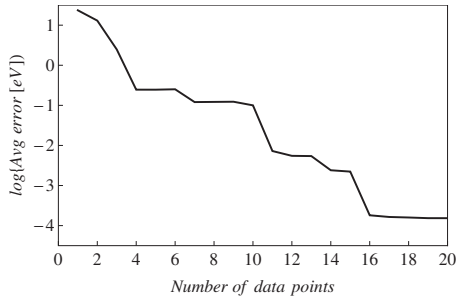

FIG. 4. The average error between the interpolated and the analytic DPEMs [$\langle\Delta\rangle$ of Eq. (4.1)] for two coupled surfaces.

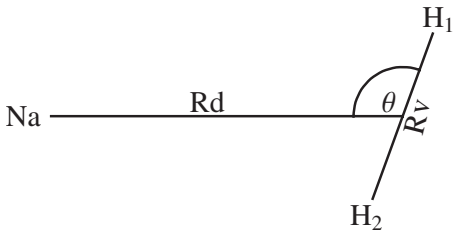

FIG. 5. The Jacobi coordinates for the $Na^*+H_2 \rightarrow Na+H_2$ process.

LEPS potential[33] V_{22} was corrected by adding a small constant to $[\cos(\sphericalangle NaH_1H_2)-\cos(\sphericalangle NaH_2H_1)]^2$, i.e., replacing it by $[\cos(\sphericalangle NaH_1H_2)-\cos(\sphericalangle NaH_2H_1)]^2+\varepsilon$, with $\varepsilon=0.168$, so that the potential drop as $\theta \rightarrow \pi/2$ is avoided (see Fig. 5).

Wave packet propagation calculations on the DPEM were performed using the MCTDH package.[16] Table I summarizes the relevant computational parameters that were used for discretizing the three Jacobi coordinates Rd, Rv, and θ and for the artificial CAPs added along the "Rd" and "Rv" degrees of freedom to avoid reflections from the grid boundaries, as well as the numbers of single particle functions and the orders of the natural expansion of the DPEM matrix using the POTFIT program.

The DPEM was calculated using the quantum grow algorithm of Sec. III. An initial set of 38 data points was prepared by selecting geometries along the minimum energy paths of the reaction on both the ground and the excited state, some geometries in the vicinity of the conical intersection, and some at the location of the initial wave function were used. In the first iterations (until the accumulation of 200 data points) the initial wave packet (step 5) was chosen to be located at the asymptotic region (large Rd). After accumulating this significant number of data points, the initial wave packet was chosen either in the asymptotic region or in the area of the conical intersection (see Table I for details), which is most relevant to the observables of interest. Since in this stage of the growing procedure each new data point would have only a minor effect on the list of most populated grid points according to Eqs. (3.2) and (3.3), the wave packet evolution (steps 4–8) was skipped in each iteration until a set of additional 20 new data points was accumulated. The convergence test for the observables (autocorrelation function and spectrum) i.e., steps 7 and 8, were performed only after every addition of 100 new data points. These observables are sensitive to the interpolated potential in the conical intersection region where the initial wave packet was localized and the main dynamical changes took place. The results in Fig. 6 show the autocorrelation spectrum with the analytic potential and with several interpolated potentials with different numbers of data points. The spectrum obtained by the interpolated potential and by the analytic potential are shown to coincide when an impressively small number of 700 data points is reached. Figure 7 depicts the drop in the potential interpolation error with increasing number of data points. Notice that the absolute error is in the range of $10^{-3}-10^{-2}$ eV, i.e., similar to the resolution of the autocorrelation spectrum. This reflects contributions to the overall error from configurations which are irrelevant to the calculated observable.

V. CONCLUSIONS

A new sampling algorithm for the interpolation of diabatic potential energy matrices by the grow method was introduced. The algorithm is based on using approximated quantum wave packet dynamics instead of classical trajectories in

TABLE I. MCTDH parameters (all units are in a.u.) V_{cut} is the cutoff-energy.

		R_d	R_v	θ	El
Grid parameters	Type	Sin	Sin	Leg	el
	N	150	60	41	2
	x_i	1.00	0.60	0	
	x_f	20.00	8.24	Even	
CAPS parameters	x_c	17.04	5.24		
	η	0.002	0.002		
	b	4	4		
POTFIT parameters for the quantum Grow procedure	V_{11}, V_{cut}=0.16	Contracted	10	10	
	V_{12}, V_{cut}=0.10	Contracted	10	10	
	V_{22}, V_{cut}=0.21	Contracted	18	10	
POTFIT parameters for the observable calculations	V_{11}, V_{cut}=0.16	Contracted	30	20	
	V_{12}, V_{cut}=0.10	Contracted	20	25	
	V_{22}, V_{cut}=0.21	Contracted	30	20	
Number of single particle functions	Ground state	12	10	10	
	Excited state	12	10	10	
Initial condition for the quantum grow procedure	Type	Gauss.	Eigenf	Leg.	
		x_0=10.5	of H_2	m=0	
		k=−3.5		l=0	
		σ=1.5	ν=1	Sym	
Initial condition for the observable calculations	Type	Gauss.	Gauss.	Gauss.	
	x_0	4.10	1.40	1.55	
	k	0.00	0.00	0.00	
	σ	0.20	0.15	0.10	

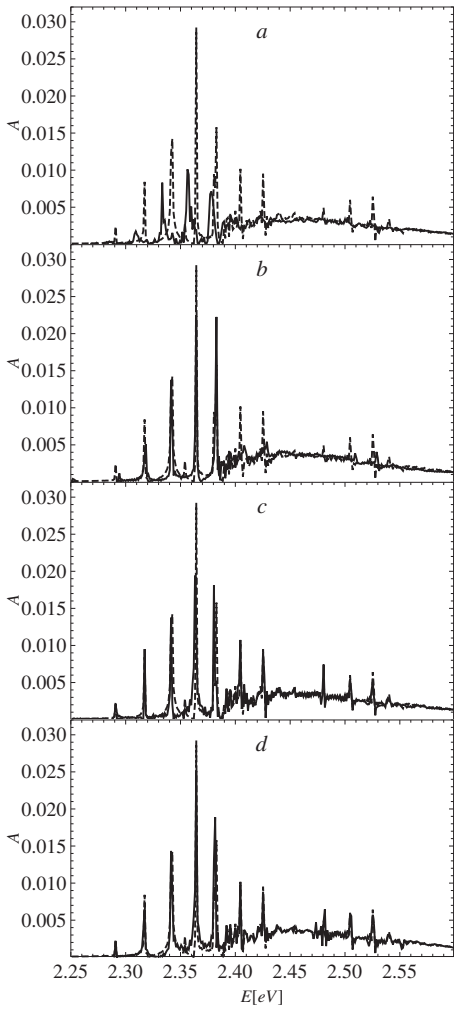

FIG. 6. Autocorrelation spectra obtained using the analytic (dashed) and the interpolated (solid) DPEMs, respectively, for the $Na^*+H_2 \rightarrow Na+H_2$ process after propagation of an initial wave packet located near the conical intersection for 900 fs. The plots a, b, c, and d correspond to 200, 400, 600, and 800 data points used for the interpolations (the model and computational parameters are listed in Table I).

order to explore the most relevant geometries for sampling the DPEM. The quantum grow procedure benefits from penetration of the wave packet into classically forbidden regions, and the accurate description of nonadiabatic transitions within the quantum dynamics. The increased complexity associated with running quantum mechanical dynamics is reduced by using approximate low order expansions of the nuclear wave function within an MCTDH scheme. The new approach was formulated and applied for three representative test cases including nonadiabatic transitions. The recovery of the relevant analytic potentials by the interpolated ones, and the convergence of the calculated autocorrelation spectra with relatively small numbers of data points, suggest that this approach may be a useful alternative to growing schemes based on purely classical dynamics.

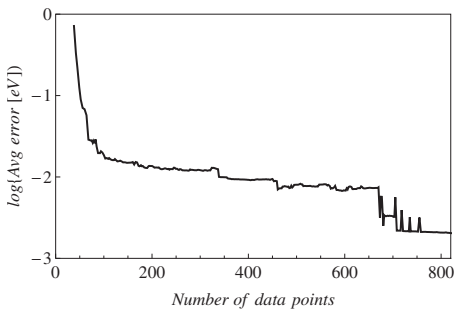

FIG. 7. The average error between the interpolated and the analytic DPEMs [$\langle\Delta\rangle$ of Eq. (4.1)] for the $Na^*+H_2 \rightarrow Na+H_2$ process.

ACKNOWLEDGMENTS

This research was supported by the German Israeli Foundation for research and development. H. Dieter Meyer is acknowledged for helpful discussions and insightful comments.

[1] J. N. Murrell, S. Carter, S. Frantos, P. Huxley, and A. J. C. Varandas, *Molecular Potential Energy Functions* (Wiley, New York, 1984), p. 206.
[2] K. B. Lipkowitz and D. B. Boyd, *Review in Computational Chemistry* (VCH, New York, 1990).
[3] R. Car and M. Parrinello, Phys. Rev. Lett. **55**, 2471 (1985).
[4] A. Lagana and A. Riganelli, *Proceedings of the European School on Computational Chemistry*, Perugia, Italy, July 1999 (Springer, Berlin, 2000), p. 312.
[5] J. Ischtwan and M. A. Collins, J. Chem. Phys. **100**, 8080 (1994).
[6] M. J. T. Jordan, K. C. Thompson, and M. A. Collins, J. Chem. Phys. **102**, 5647 (1995).
[7] K. C. Thompson, M. J. T. Jordan, and M. A. Collins, J. Chem. Phys. **108**, 8302 (1998).
[8] R. P. A. Bettens and M. A. Collins, J. Chem. Phys. **111**, 816 (1999).
[9] C. R. Evenhuis and M. A. Collins, J. Chem. Phys. **121**, 2515 (2004).
[10] C. R. Evenhuis, X. Lin, D. H. Zhang, D. R. Yarkony, and M. A. Collins, J. Chem. Phys. **123**, 134110 (2005).
[11] O. Godsi, C. R. Evenhuis, and M. A. Collins, J. Chem. Phys. **125**, 104105 (2006).
[12] M. A. Collins, Theor. Chem. Acc. **108**, 313 (2002).
[13] G. A. Worth, M. H. Beck, A. Jackle, and H.-D. Meyer, The MCTDH package, Version 8.2, 2000; H.-D. Meyer, The MCTDH package, Version 8.3, 2002, (see: http://www.pci.uni-heidelberg.de/tc/usr/mctdh/).
[14] H.-D. Meyer, U. Manthe, and L. S. Cederbaum, Chem. Phys. Lett. **165**, 73 (1990).
[15] U. Manthe, H.-D. Meyer, and L. S. Cederbaum, J. Chem. Phys. **97**, 3199 (1992).
[16] M. H. Beck, A. Jackle, G. A. Worth, and H.-D. Meyer, Phys. Rep. **324**, 1 (2000).
[17] H.-D. Meyer and G. A. Worth, Theor. Chem. Acc. **109**, 251 (2003).
[18] T. Wu, H.-J. Werner, and U. Manthe, Science **306**, 2227 (2004).
[19] R. van Harrevelt, K. Honkala, J. K. Nørskov, and U. Manthe, J. Chem. Phys. **122**, 234702 (2005).
[20] T. Wu and U. Manthe, J. Chem. Phys. **119**, 14 (2003).
[21] M. Baer, Chem. Phys. Lett. **35**, 112 (1975).
[22] R. G. Sadygov and D. R. Yarkony, J. Chem. Phys. **109**, 20 (1998).
[23] C. A. Mead and D. G. Truhlar, J. Chem. Phys. **77**, 6090 (1982).
[24] *Conical Intersections: Electronic Structure, Dynamics and Spectroscopy*, edited by W. Domcke, D. R. Yarkony, and H. Köppel (World Scientific, Singapore, 2004).
[25] G. A. Worth and L. S. Cederbaum, Annu. Rev. Phys. Chem. **55**, 127 (2004).
[26] J. C. Tully, J. Chem. Phys. **93**, 1061 (1990).
[27] In these examples the steps requiring *ab initio* inputs were skipped and steps (1)–(3) of the general algorithm were replaced by: (1) chose initial data points; (2) go to step 3; and (3) calculate the DPEM for a discrete representation in a selected coordinate system.
[28] R. Kosloff and D. Kosloff, J. Chem. Phys. **79**, 1823 (1983).

[29] M. D. Feit, J. A. Fleck, Jr., and A. Steiger, J. Comput. Phys. **47**, 412 (1982).
[30] W. Zrafi, B. Oujia, and F. X. Gadea, J. Phys. B **39**, 3815 (2006).
[31] D. W. Schwenke, S. L. Mielke, G. J. Tawa, R. S. Friedman, P. Halvick, and D. G. Truhlar, Chem. Phys. Lett. **203**, 565 (1993).
[32] R. J. Duchovic, Y. L. Volobuev, G. C. Lynch, A. W. Jasper, D. G. Truhlar, T. C. Allison, A. F. Wagner, B. C. Garrett, J. Espinosa-García, and J. C. Corchado, POTLIB, http://comp.chem.umn.edu/potlib.
[33] In the present work the NaH_2 surface set 7 s from POTLIB was used, based on unpublished work of M. D. Hack and D. G. Truhlar (2000).
[34] H.-J. Werner, P. J. Knowles, R. Lindh *et al.*, MOLPRO, version 2008.3, University of Birmingham, UK, 2008.